Uncertainty Analysis of Reflection Coefficient for a Coating with Random Flaws Using Adaptive Mesh and DGTD Method

Huiping Li [1,2], Ishfaq Hussain [1], Yi Wang [1], and Qunsheng Cao [1]

[1] College of Electronic and Information Engineering
Nanjing University of Aeronautics and Astronautics, Nanjing, 211106, China
lihp@nuaa.edu.cn, ishfaqhussain05@nuaa.edu.cn, jflsjfls@nuaa.edu.cn, qunsheng@nuaa.edu.cn

[2] School of Physics and Electronics
Henan University, Kaifeng 475004, China

Abstract ─ An imperfect coating shall cause uncertainties in the analysis of electromagnetic properties. To quantify the influence of irregularity, complexity, and uncertainty of the coatings for electronic devices, an adaptive mesh algorithm combined with the discontinuous Galerkin time domain (AM-DGTD) method is developed. The uncertain variations are incorporated into the proposed algorithm by an appropriate parameterization. The standard statistical analysis is performed to calculate the appropriate moments, i.e., mean and variance. The developed method is validated by modeling a dielectric coating with uncertain flaws in an adaptive mesh grid. The computed quantities of interest from numerical estimations are compared with the analytical values, these results agree with the physical explanation, and are in good agreement with the exact values, as demonstrated by numerical experiments.

Index Terms ─ AM-DGTD method, reflection coefficient, statistical analysis, uncertainty quantification.

I. INTRODUCTION

Dielectric coatings applied to surfaces of aircraft frames, automobile frames and ship hull are able not only to protect objects from sunlight, moisture, dust and abrasion but also to improve their appearance [1]. For example, cracks, voids, inclusions, structural flaws and material defects [2], these uncertain flaws may impact the coating's electromagnetic performance and cause difference from the ideal manufacturing objectives, or to damage the essential functions of the dielectric coatings. In order to engage in the practical analysis and simulation, one must find a suitable, flexible and efficient method to deal with these electromagnetic problems.

In the recent years, the method of moments (MoM) with probabilistic technique outlined in [3] was applied to determine the uncertainty in practical EM compatibility measurements. Polynomial chaos technique was used in the finite difference time domain (FDTD) method to study microwave circuits and free-space scattering problems [4]-[5]. An efficient stochastic finite difference time domain (S-FDTD) method [6], which uses truncated Taylor series approximations in the derivation, is employed for evaluating statistical variation in the EM fields caused by variability or uncertainty in the electrical properties of the materials in the model. To obtain static response characteristics of graphite/epoxy composite laminates with random material properties, Navaneetha Raj *et al.* employed Monte Carlo simulation and the finite element method (FEM) with different boundary conditions [7]. A hybrid approach was adopted in the spectral stochastic finite element method (SSFEM) and polynomial chaos expansion (PCE) to provide response analysis of a linear structure with uncertainties in both the structural parameters and the external excitation [8]. In [9], a probabilistic approach based on high-order accurate expansions of general stochastic processes and high-order discontinuous Galerkin method was applied to solve the time-domain electromagnetic problems with uncertainty in initial conditions, boundary conditions, sources, materials, computational domain, and/or geometries. In [10], Li *et al.* proposed a hybrid method which integrated an adaptive hierarchical spare grid collocation (ASGC) method and the discontinuous Galerkin time-domain (DGTD) method. The ASGC method is employed to approximate the stochastic observables of interest using interpolation functions over a set of collocation points determined by the Smolyak's algorithm integrated with an adaptive strategy. Owing to the random flaws in the coatings are generally smaller, irregular, and more arbitrary in nature. Moreover, the DGTD method offers high-order accuracy to a coarse resolution, geometrical flexibility through fully unstructured grids and higher computational efficiency, so it could be more suitable to be employed for the uncertainty quantization [9]-[14].

In this work, using the node displacement method and the node insertion method[15]-[17], we develop an

Submitted On: August 9, 2017
Accepted On: January 22, 2018

adaptive spatial discrete algorithm for the high order DGTD method to generate an optimal number of mesh elements and to adapt the locations of the global nodes for uncertain and complex structures. The AM-DGTD method is used to evaluate the statistical variations of reflection coefficients of dielectric coating with random flaws in one-dimensional model. Firstly, we compare the high-order convergence of the AM-DGTD algorithm for different values of the number of element K and the order of polynomial N. Then, we solve three typical uncertain flaw problems using the developed approach: (i) slight deviation in the permittivity of the dielectric coating, (ii) variable tolerance in the thickness of coating, and (iii) uncertain holes in the coating. For the first two cases, there is only one uncertain input parameter, i.e., permittivity and thickness, respectively. For the third case, we investigate multivariable situation, e.g., the diameter, position, and number of holes as the stochastic variables. Furthermore, this article not only provides results of uncertainties but also insight into the expected statistical properties.

II. ADAPTIVE MESH DGTD METHOD

To use unstructured finite element methods, the computational domain must be decomposed into geometric elements, e.g., lines in one dimension, triangles in two dimensions and tetrahedral in three dimensions. Suppose one-dimensional computational domain is $\Omega = [xmin, xmax]$, which can be tessellated by K equidistant nodes. If the meshes are uniform then each element has the same size $h = \Omega/K$. When the desired nodes, which represent the interfaces of the structure under study, do not coincide with the positions of the equidistant nodes, the uniform meshes are terrible and unserviceable. If setting a larger h, the discretization error will increase; if setting a smaller h for capturing fine details and maintaining Courant-Friedrichs-Levy (CFL) condition of the numerical methods, the computational memory and execution time will increase.

For problems with uncertain desired nodes, dynamic, intelligent, and more robust meshes are needed to achieve accurate identification for the random objects. In this work, two types of adaptive mesh generation techniques are proposed as below:

A. Node insertion mesh

Firstly, the computational domain Ω is discretized into K equidistant non-overlapping line segments. Each line segment has two end nodes. Vx is introduced to stand for the global uniform node vector (UNV). Using the insertion algorithm, the desired node vector (DNV) can be added adaptively into UNV and the resulting vector is sorted to achieve overall discretization scheme. The new global node vectors could become nonuniform. Note that the number of global nodes is increased as inserting DNV, as shown in Fig. 1.

The node insertion method is simple, however, it is time and resource-consuming, because the insertion of DNV into V_x cause reduction in the minimum distance between adjacent nodes, then the smaller time step has to be employed to maintain the CFL condition. Pseudo algorithm for this adaptive mesh by inserting node is provided in Algorithm 1.

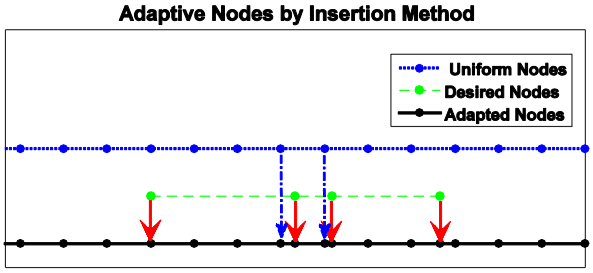

Fig. 1. The mesh cell mappings for node inserting mesh algorithm.

Algorithm 1 Insertion algorithm for desired nodes

Input: computational domain Ω=[*xmin*, *xmax*], number of elements K, desired node vectors *DNV*
Output: updated number of elements K*, updated global node vector V_x*

for i←1 to K do
  /* Generate a simple equidistant grid and uniform node vectors V_x */
  V_x(i) ← (*xmax*−*xmin*)*(*i*-1)/K + *xmin*
/* Insert the *DNV* into the uniform node vector V_x */
/* Sort and return the unique values */
V_x*←unique ([V_x *DNV*])
K*←length(V_x*)-1
Return K*, V_x*

B. Node displacement mesh

In this type of adaptive mesh generation, the adaptation can be achieved through suitably displacing the UNV. The algorithm identifies the nodes from the UNV which are nearest to the set of DNV and shifts these nodes to the desired locations. If a DNV coincides with one of the UNV, such as the node ① and ②, then no displacement is needed; if a structure represented by any two of the DNV (e.g., node ② and ③) is much larger than uniform elements, then the nearest uniform nodes are modified at the boundaries; if a structure is very small, such as the segment composed by node ⑤ and ⑥, the algorithm makes sure that at least one element is contained. Hence, only optimal numbers of element are generated, as shown in Fig. 2.

Note that the number of global nodes remains unchanged, that is, K* = K. This algorithm generates optimal density of mesh cells over the whole Ω,

regardless of geometry structure. The displacement of nodes to different position caused non-uniformity in the distribution of global nodes. Realization for this adaptive mesh algorithm is given below in Algorithm 2.

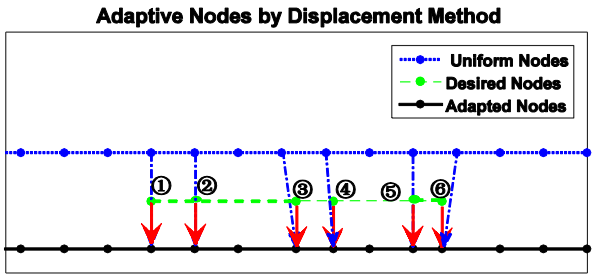

Fig. 2. The mesh cell mappings for node displacing mesh algorithm.

Algorithm 2 Displacement algorithm for desired nodes

Input: computational domain Ω=[*xmin*, *xmax*], number of elements *K*, desired node vectors *DNV*
Output: updated number of elements *K**, updated global node vector V_x*

```
for i←1 to K do
    /* Generate a simple equidistant grid and uniform
       node vectors Vx */
    Vx(i) ← (xmax−xmin)*(i-1)/K + xmin
if length(Vx) > 2*length(DNV)+2 then
    for q← 1 to length(DNV) do
        /*Generate index of DNV in set of the uniform
          node vectors UNV */
        [Val(q) Index(q)] ← min(abs(Vx−DNV(q)))
        /* Deal with nodes which near boundary of
        the domain */
        ConflictIndex ← find( Index(end)==Index)
            if length(ConflictIndex) > 1 then
                Index(end) ← Index(end)+1
            return
        Vx (Index(q)) ← DNV(q)
    Vx*←Vx
    K*←length(Vx*)-1
return
Return K*, Vx*
```

C. Numerical scheme for one-dimensional case

To compute the reflection coefficients of the dielectric coating with random flaws, we solve the one-dimensional Maxwell's equations in the time domain, subject to a broadband initial condition, and collect one time-trace at an observed point in the computational domain. Consider a lossless material TEM_z case, the time-dependent Maxwell's equations can be written as follows:

$$\varepsilon(z)\frac{\partial E_x}{\partial t}+\frac{\partial H_y}{\partial z}=0,\qquad \mu(z)\frac{\partial H_y}{\partial t}+\frac{\partial E_x}{\partial z}=0, \tag{1}$$

where E_x, H_y, ε and μ represent the electric field, the magnetic field, the local electric permittivity, and the local magnetic permeability, respectively.

Using the aforementioned adaptive mesh approaches, the computational domain $\Omega = [l, r]$, which is tessellated by K^* subdomains, i.e., any one of elements of the physical space D^k is equal to $[z_l^k, z_r^k], k = 1...K^*$. The solution of Equation (1) will be discontinuous between elements. In an arbitrary element D^k, the fields can be approximately expanded using local high-order Lagrange interpolation polynomial $\ell_i^k(z)$:

$$\begin{bmatrix}E_x^k(z,t)\\H_y^k(z,t)\end{bmatrix}\approx\begin{bmatrix}E_{xh}^k(z,t)\\H_{yh}^k(z,t)\end{bmatrix}=\sum_{i=1}^{N_p}\begin{bmatrix}E_{xh}^k(z_i^k,t)\\H_{yh}^k(z_i^k,t)\end{bmatrix}\ell_i^k(z), \tag{2}$$

where N_p stands for the number of the local expansion. E_{xh}^k and H_{yh}^k contain a N_p-vector of expansion coefficients to be solved. $\ell_i^k(z)$ signifies an N_pth order Lagrange polynomial. The relationship between N_p and the polynomial expansion order N is $N_p = N+1$. On account of the fact that correctly choosing interpolation nodes can bring about good numerical behaviors, this work employs the Legendre-Gauss-Lobatto (LGL) interpolating nodes as z_i [21]-[23].

Next, multiplying (1) by a test function $\ell_i^k(z)$ in an element D^k, yields:

$$\begin{aligned}&\int_{D^k}\left(\varepsilon^k(z)\frac{\partial E_x^k(z,t)}{\partial t}+\frac{\partial H_y^k(z,t)}{\partial z}\right)\ell_i^k(z)\,dz=0,\\&\int_{D^k}\left(\mu^k(z)\frac{\partial H_y^k(z,t)}{\partial t}+\frac{\partial E_x^k(z,t)}{\partial z}\right)\ell_i^k(z)\,dz=0.\end{aligned} \tag{3}$$

In order to couple with adjacent elements, Equation (3) are manipulated with integration by parts twice, and the strong variational formulation can be obtained as [21]:

$$\begin{aligned}&\int_{D^k}\left(\varepsilon^k\frac{\partial E_x^k}{\partial t}+\frac{\partial H_y^k}{\partial z}\right)\ell_i^k(z)\,dz=\int_{\partial D^k}\hat{\boldsymbol{n}}\cdot\left(\frac{\partial H_y^k}{\partial z}-\frac{\partial H_y^*}{\partial z}\right)\ell_i^k(z)\,dz,\\&\int_{D^k}\left(\mu^k\frac{\partial H_y^k}{\partial t}+\frac{\partial E_x^k}{\partial z}\right)\ell_i^k(z)\,dz=\int_{\partial D^k}\hat{\boldsymbol{n}}\cdot\left(\frac{\partial E_x^k}{\partial z}-\frac{\partial E_x^*}{\partial z}\right)\ell_i^k(z)\,dz.\end{aligned} \tag{4}$$

Here, $\hat{\boldsymbol{n}}$ denotes the local outward pointing normal. On the right-hand side (RHS) of (4) (E_x^*, H_y^*) are numerical fluxes to exchange the coupling between neighboring elements. Using the Riemann conditions

and for stability reasons, we use a pure upwind flux [21] which could strongly damp unphysical modes,

$$E_x^* = \frac{1}{\{\{Y\}\}}\left(\left\{\left\{YE_x^k\right\}\right\} + \frac{1}{2}[[H_y^k]]\right)$$
$$H_y^* = \frac{1}{\{\{Z\}\}}\left(\left\{\left\{ZH_y^k\right\}\right\} + \frac{1}{2}[[E_x^k]]\right), \quad (5)$$

where $Z = (Y)^{-1} = \sqrt{\mu/\varepsilon}$, represents the impedance of the medium.

Now substitute the expansions in (2) with the numerical flux of (5) into (4) and assume a smooth material in each element. After some algebraic computations, the explicit semi-discrete scheme in matrix-vector form can be obtained as follows:

$$\frac{dE_{xh}^k}{dt} = \frac{1}{J^k\varepsilon^k}\left\{-\mathcal{D}_r H_{yh}^k + \frac{1}{\mathcal{M}^k}\left[\ell^k(z)\left(H_{yh}^k - H_y^*\right)\right]_{z_l^k}^{z_r^k}\right\},$$
$$\frac{dH_{yh}^k}{dt} = \frac{1}{J^k\mu^k}\left\{-\mathcal{D}_r E_{xh}^k + \frac{1}{\mathcal{M}^k}\left[\ell^k(z)\left(E_{xh}^k - E_x^*\right)\right]_{z_l^k}^{z_r^k}\right\}. \quad (6)$$

Here, the matrices J^k, D_r, and M^k represent the local transformation Jacobian, differentiation matrix and mass-integration matrix, respectively (see [21] for details).

The semi-discrete system of (6) is ordinary differential equations with respect to time. The forth-order low-storage explicit Runge-Kutta (LSERK) solver is employed for the time integration of (6) [24].

III. AM-DGTD FOR DETERMINISTIC PARAMETERS

A. Computation model

The objective of this article is to analyze the characteristics of a dielectric coating. To reduce the complexity of the problem, this coating is located at the center (i.e., $x^{left} = 0$) of the computational domain Ω = [-6.0cm, 6.0cm]. Free space is set on the both sides of the coating and the relative parameters $\varepsilon_r = 1$ and $\mu_r = 1$. The main sensitive variables with uncertainty are supposed to be mean values, i.e., the average thickness of the coating d = 2.0cm and its average relative permittivity $\varepsilon_r = 4$.

To model the excitation source, an x-polarized, z-directed Gaussian pulse with respect to space is used and the following initial conditions ($t=0$) are adopted as:

$$E_x = \exp\left(-4\pi\frac{(z-z_0)^2}{z_\tau^2}\right),\ z_0 = -3.5cm, z_\tau = 0.5cm$$
$$H_y = 0 \quad (7)$$

where z_0 and z_τ are the center position and the width of the Gauss curve, respectively. This Gaussian pulse traveling in free space normally incident upon the dielectric coating, as illustrated in Fig. 3.

We collect one time-trace at the observation point (P = -1.0cm) in the computational domain. The frequency response is obtained by using fast Fourier transformation (FFT). Moreover, the Mur's absorbing boundary conditions (ABC) [25] is employed to truncate the open domain.

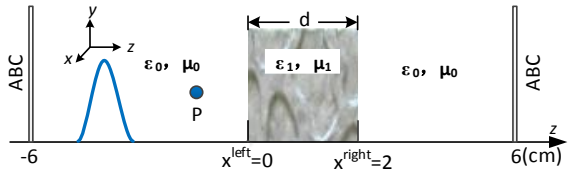

Fig. 3. The sketch map of the dielectric coating with uncertain flaws.

B. Reflection coefficient

The reflection coefficients at the observation point are calculated by using the AM-DGTD method. The coating is assumed to be removed at first, that is, the whole computational domain lies in free space. The electric field data at the observation point can completely represent the incident field, E^{inc}. Then, the complete model is simulated again. Because of the discontinuous interface, when the incident wave encounters the interface, a fraction of the wave energy will be reflected and part will be transmitted. Hence, the electric field data at the same observation point represents the total field E^{tot}, which includes incident and reflected electric field components. The formulation for the reflected fields is given by $E_x^{ref} = E_x^{tot} - E_x^{inc}$. Figure 4 illustrates the relationship of incident, total, and reflected electric field with time at the observation point.

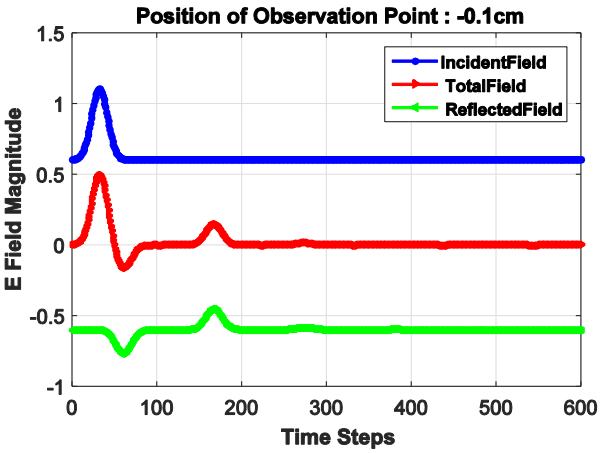

Fig. 4. The relationship of incident, total, and reflected electric field.

Using FFT, the frequency responses of the incident and reflected electric fields are obtained, then the reflection coefficients $\Gamma = E^{ref}/E^{inc}$ are achieved.

When uncertain parameters impact on the computational model, supposing θ is independent random

parameter with probability density function (PDF). The random parameter may come from uncertain material parameters, geometrical shapes, boundary conditions, initial conditions, computational domain, etc. To model the impact of these randomness and uncertainty on the propagation of EM waves, the solution of E^{inc} and E^{ref} can be expressed as $E^{inc}(z,t,\theta)$ and $E^{ref}(z,t,\theta)$, they are not only a function of (z, t) but also of θ. Therefore, the reflection coefficient Γ are uncertain and stochastic, correspondingly. The statistical moments of the solutions, such as mean and variance of Γ can be quantified [18]-[20] as:

$$E[\Gamma]=\frac{1}{M}\sum_{m=1}^{M}\Gamma_m$$

$$Var[\Gamma]=E[(\Gamma-E[\Gamma])^2]=\frac{1}{M}\sum_{m=1}^{M}(\Gamma_m-E[\Gamma])^2, \quad (8)$$

$$Std[\Gamma]=\sqrt{Var[\Gamma]}$$

$$CI[\Gamma]:\left(E[\Gamma]-n\cdot Std[\Gamma],E[\Gamma]+n\cdot Std[\Gamma]\right)$$

where M represents the samples of the stochastic parameters, which are generated by using a random number generator. $E[\Gamma]$ stands for the mean of the random variable Γ; $Var[\Gamma]$ and $Std[\Gamma]$ are the variance and standard deviation of the random variable Γ, respectively; $CI[\Gamma]$ denotes the confidence interval with an upper and lower bounds. The n is used as the critical value. This value is only dependent on the confidence level of the test. A typical two-sided confidence level is as n = 1.96, which corresponds to the confidence interval as 95% (see [18] for details).

C. Results and analysis

To validate the approach discussed above, the reflection coefficients are calculated by the AM-DGTD method for the sensitive variables given. The constitutive parameters are the same as in Subsection A.

Figure 5 plots the computed solution at final time T = 10s as a function of the number of adaptive elements, K, and the order of the local approximation, N. Comparing with analytic solutions, it shows a good agreement for different parameter sets (N, K). There are two ways to improve the accuracy of Γ: (i) keep N fixed, and increase K, known as h-refinement, and (ii) keep K fixed, and increase N, known as order or p-refinement [21]. As shown in the magnified image at around 1.85 GHz, simulation results using larger N or K are closer to analytic results.

Figure 6 shows the results of absolute errors (compared to analytic results). The errors decay fast with increasing N or K, while both lead to a better approximation. Because of smaller errors at the extreme points, there is better manner at the maximum and minimum of the reflection coefficient Γ, i.e., at 1.85 GHz and 3.75 GHz. But with increasing frequency, the error values become somewhat large.

Inspecting results in Fig. 6, one observes that the results of AM-DGTD scheme are clearly convergent for increasing K and/or N. However, the high accuracy comes at a price. The higher accuracy needs the greater execution time. Table 1 has listed the root mean square (RMS) error and the execution time at different combinations of (N, K). Consider, as an example, an error of O (3.0e-5). From the results in Table 1, we see that this can be achieved through (2, 40), (2, 160), (3, 40), and (4, 20) (the bold font). Comparing with these results, the combination of (2, 40) has the highest order of approximation and the fastest running time in which the hosting CPU is Intel Core i3-4150 with four cores and clock speed of 3.5 GHz.

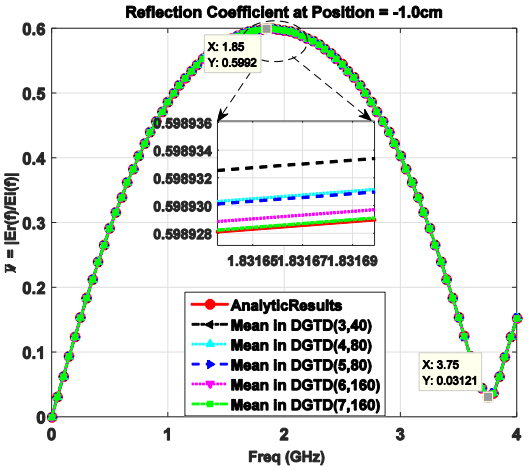

Fig. 5. The reflection coefficient for different sets of parameters (N, K) compared against the exact solution.

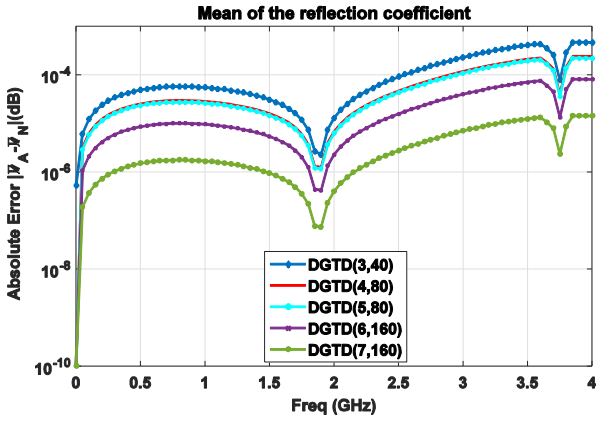

Fig. 6. Absolute errors for different sets of parameters (N, K) compared against the exact solution.

Because the stochastic problems require generally a large number of the variables to calculate statistical properties, one must make a trade-off between accuracy and execution time for the employed method. According

to the results of Table 1, the combination of (N, K) = (2, 40) has been chosen, because of its higher accuracy and lesser time.

To analyze execution time efficiency, an ultra-thin coating is handled by the AM-DGTD method. Comparing with traditional DGTD method, the AM-DGTD approach can save more execution time. For example, when the thickness of the ultra-thin coating is 0.05cm, the execution time is 1724.4648s and 205.0989 s, respectively, using the traditional DGTD and the AM-DGTD methods. It is clearly exhibiting that the AM-DGTD technique helps achieving very fast numerical computations.

Table 1: RMS error (GHz), total execution time (s)

N \ K	20	40	80	130	160
1	5.3615e-3	1.1319e-3	2.8409e-4	1.0901e-4	7.1152e-5
	5.1219	6.4955	10.0083	14.0528	16.5547
2	1.8919e-3	**2.4724e-5**	5.1515e-5	1.4265e-5	**2.7230e-5**
	6.5837	**9.6089**	16.4490	24.8534	**30.1344**
3	5.3715e-5	**2.7734e-5**	1.9115e-5	2.0471e-5	1.2255e-5
	9.1618	**15.0469**	26.7811	42.7873	52.5584
4	**3.0970e-5**	2.3152e-5	2.0652e-5	1.3980e-5	1.2212e-5
	12.5116	21.9100	41.4415	67.3585	82.5465
5	2.4773e-5	1.3339e-5	1.3075e-5	1.5433e-5	1.3684e-5
	17.1342	30.7708	59.2901	97.0274	120.9001
6	3.1082e-5	1.7996e-5	1.5677e-5	1.4709e-5	1.2306e-5
	22.2469	41.6919	81.7953	134.7709	167.9819
7	1.6191e-5	1.9432e-5	1.3092e-5	1.3431e-5	1.3097e-5
	28.1425	54.0226	106.8370	176.5143	220.7351

IV. AM-DGTD FOR STOCHASTIC PARAMETERS

The actual form of flaws in the dielectric coating may not be known, causing the introduction of the uncertainty in some sensitive parameters. These uncertainties can be based on pure speculation, on measured data, or on other available information. In this section, a few typical uncertain flaws are discussed and validated by the AM-DGTD approach. To reduce the complexity of the simulations, the uncertain flaws are expressed as stochastic variables, characterized with appropriate probability distributions. And these stochastic variables are statistically independent.

A. Uncertainty in material

Deterministic solutions require accurate input parameters, however, there always exist uncertain material properties such as from imprecise measurement or manufacturing. In this section, the case of uncertainty in permittivity is considered, that is, tolerances and uncertainties lie in the relative permittivity ε_r.

For the model in Fig. 3, a randomness in the relative permittivity of the dielectric coating is assumed as [9]:

$$\varepsilon_r(x,\theta)=\begin{cases}1 & x\notin coating\\ 4\cdot\left(1+\dfrac{0.1\cdot\theta^2}{1+\theta^2}\right) & otherwise\end{cases}, \tag{9}$$

where θ is a Gaussian variable with zero mean and unit variance. With the uncertainty of the formula (9), the relative permittivity ε_r is guaranteed to remain positive in the domain of the dielectric coating. Note that our concern is not the correctness of the probabilistic law chosen in (9) for the uncertainty of the ε_r, since for any reasonable law, the techniques presented in this paper should work equally well.

Other parameters are fixed as the computational domain Ω = [-6.0cm, 6.0cm], the thickness of the coating d = 2.0cm, the position of the observed point P = -0.1cm, the total computational time T = 10s.

The mean and standard deviation of the reflection coefficient Γ of have been evaluated by the AM-DGTD method at the observation point. Table 2 shows the results of the quantitative uncertainties of the Γ versus different tolerances of the relative permittivity ε_r, i.e., the minimum, maximum, mean and 95% confidence intervals (CI) of Γ at the maximum 1.85 GHz. With the increasing of the $\Delta\varepsilon_r$, it has been found that the $E[\Gamma]$ is far away from the value of $\Delta\varepsilon_r = 0$. When the $\Delta\varepsilon_r$ is negative, i.e., the value of ε_r turns small, the $E[\Gamma]$ is reduced and the region of 95% $CI[\Gamma]$ widens, e.g., ε_r = 3.8612, then $E[\Gamma]$ = 0.5878, $CI[\Gamma]$ = [0.5690, 0.6067]. On the contrary, the $\Delta\varepsilon_r$ is positive, i.e., the value of ε_r turns big, the $E[\Gamma]$ is increased and the region of 95% $CI[\Gamma]$ also widens, e.g., ε_r = 4.2994, then $E[\Gamma]$ = 0.6214, $CI[\Gamma]$ = [0.5924, 0.6505].

To study the relationship of the deviation of reflection coefficient Γ and permittivity ε_r, another 1000 independent random variables are used. The results of uncertainty quantification of reflection coefficient with different deviations in permittivity ε_r over a 0-4 GHz frequency range are shown in Fig. 7. It is obvious that the minimum

reflection point, i.e., 3.75 GHz, turn worse with the tolerances of ε_r increase. When the tolerance of ε_r is changed, the value of this point is increased, i.e., the value of ε_r decreases, this point shifts a bit to higher frequency; when the values of ε_r increases, the point shifts a bit to lower frequency. The increased offset indicates an increased tolerance existing in the results.

Table 2: Uncertainty quantification of Γ versus different deviation in ε_r

$\Delta\varepsilon_r$ \ Γ	Min	Max	Mean	95% CI
-0.4056	0.4737	0.5999	0.5595	[0.4905, 0.6286]
-0.2831	0.5287	0.5999	0.5735	[0.5311, 0.6159]
-0.1388	0.5681	0.5999	0.5878	[0.5690, 0.6067]
0.0	0.5999	0.5999	0.5999	[0.5999, 0.5999]
0.1287	0.5999	0.6267	0.6098	[0.5943, 0.6253]
0.2994	0.5999	0.6474	0.6214	[0.5924, 0.6505]
0.4232	0.5999	0.6668	0.6286	[0.5882, 0.6690]

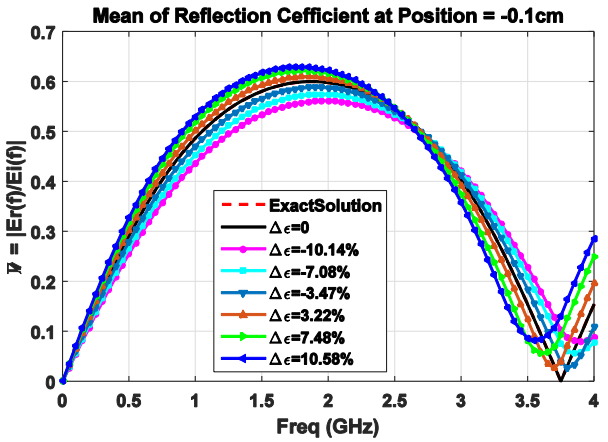

Fig. 7. Distribution of Γ with respect to different deviation in ε_r.

B. Uncertainty in thickness of coating

Suppose that the physical thickness of the dielectric coating is unknown, i.e., when there is uncertainty associated with the position of the right boundary of the coating. Uncertainty in the thickness of d can be modeled by choosing x^{right} a random variable and keeping x^{left} as constant. And the randomness x^{right} is a random parameter with some associated PDF.

The uncertain deviation in the right boundary position is chosen, so that the thickness of the coating is of variable value. The position of the right boundary is assumed to be $x^{right} = d + g(\theta)$, this allows x^{right} to be positioned on both sides of the mean position. Here $g(\theta)$ (the deviation in thickness Δd) is a uniform variable. The mean is chosen as ±0.1, ±0.2 and ±0.3 with a tolerance of ±0.01, i.e., $g(\theta)/\Delta d$ is uniformly distributed in the interval [±0.09cm, ±0.11cm], [±0.19cm, ±0.21cm], and [±0.29cm, ±0.31cm], respectively.

Figure 8 shows how the uncertain deviation in thickness of the dielectric coating affects the reflection coefficient Γ at the observation point P = -0.1cm, which are computed using the AM-DGTD formulation outlined in Section III. In the frequency 0-5 GHz range, the magnitude of the mean of Γ for 1000 samples of the random thickness is shown in the Fig. 8. When Δd = 0, the numerical results are in good agreement with analytic solutions. With the thickness d decreasing, e.g., the average thickness is from 2.3cm to 1.7cm, it has been observed obviously that the curves of the reflection coefficient Γ are extended towards the x axis and the minimum reflection frequency points shift from low to high frequency.

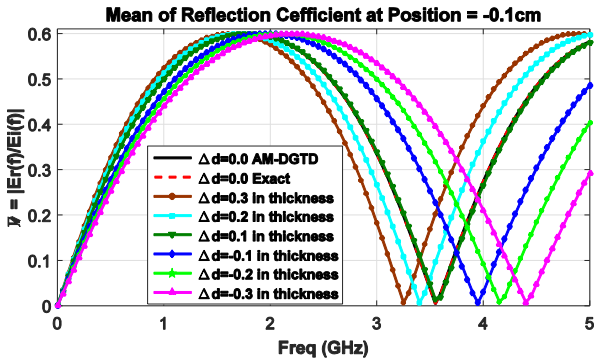

Fig. 8. Mean of Γ for 1000 samples drawn from the AM-DGTD simulations.

C. Random holes in coating

In this experiment, the AM-DGTD method is employed to analyze the reflection coefficients of imperfect dielectric coating caused by blotch, bubble, or recessed hole on a film. The different number, different radius, and random positions of holes in the dielectric coating of the range of [0.0cm, 2.0cm] are simulated.

1) Single hole

The hole parameters are assumed as ε_{rh} = 1, μ_{rh} = 1. The arbitrary mesh is represented in Fig. 9, the radius and random position of the hole are statistically independent. The number of the elements is set as K = 40. Degrees of two (N = 2) polynomials are enough to ensure that convergence is achieved in the physical space. The randomness of the holes can be incorporated into the AM-DGTD method by introducing uncertainty in the local computational mesh. To accomplish this, a displacement mesh is employed around each uncertain portion of the geometry.

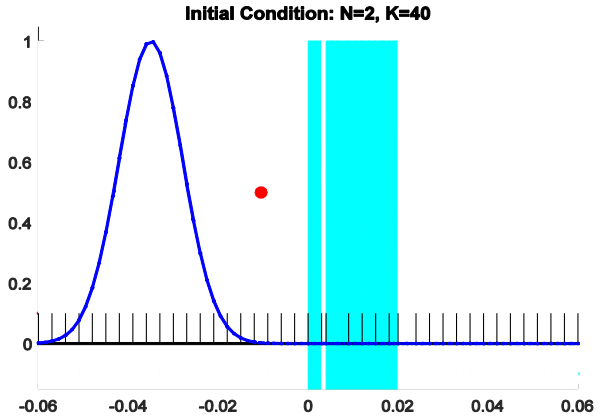

Fig. 9. The sketch of the model with one uncertain hole.

Three cases with random position and radius r as 0.025cm, 0.05cm, and 0.1cm are considered, respectively. Comparisons of the mean of the reflection coefficient Γ with and without these random holes over a 0-10 GHz frequency range are presented in Fig. 10. When the radius r is increased, the mean Γ becomes worse. For instance, the maximum reflection coefficient at 1.85 GHz is decreased, and the minimum value at 3.75 GHz is increased. And the curves of frequency-domain response are shifted a bit to higher frequency.

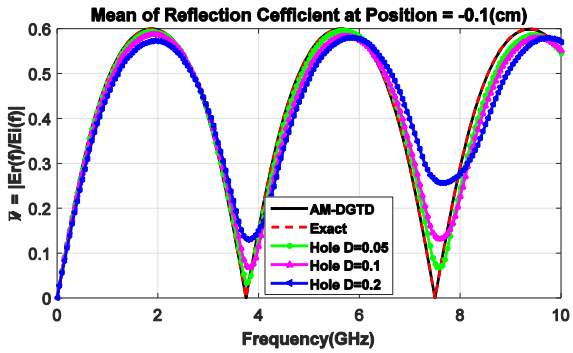

Fig. 10. One hole with random positions and variable diameter.

2) Multiple holes

An arbitrary mesh with two uncertain holes is represented in Fig. 11, all parameters are same as that of single-hole case. With the increasing of hole radius, the mean of reflection coefficient Γ becomes worse. For example, the value of the maximum becomes smaller and the value of the minimum becomes bigger.

The properties of results are similar to those of the single-hole case, but for the two random holes, the curve shifts more bit to the higher frequency, as shown in Fig. 12. The comparison results of the mean of the reflection coefficient of the model with 0-3 random holes are summarized in Fig. 13. It has been found that the mean Γ becomes worse with the number of the holes increasing.

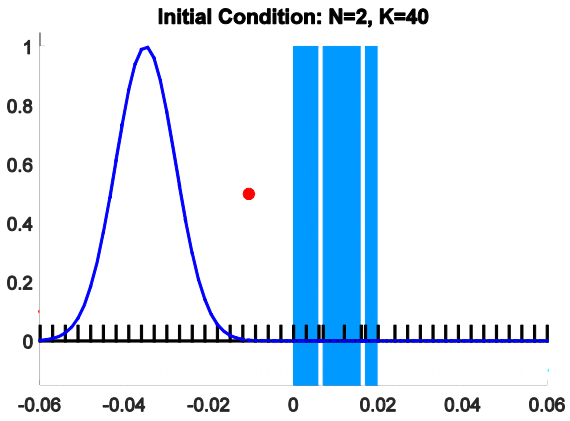

Fig. 11. The sketch of the model with two uncertain holes.

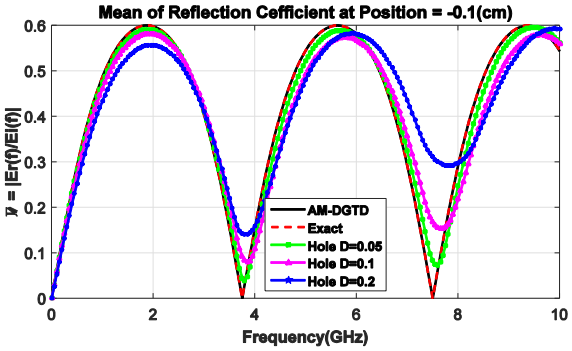

Fig. 12. Two holes with random positions and variable radius.

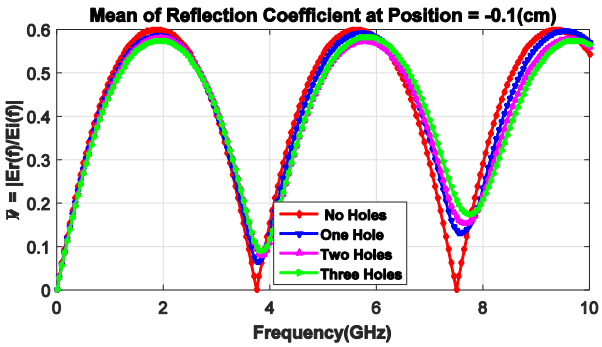

Fig. 13. Comparison of the Γ for different numbers of random hole.

Figure 14 shows the estimation of mean Γ and 95% *CI* for the imperfect dielectric coating with random number of holes computed by the AM-DGTD method. And the radius of hole is supposed to equal to 0.1cm, and the positions of hole are randomly selected. The limits of the 95% *CI* are obtained from the PDF, such that

the 2.5% of the data goes beyond the lower and upper bounds, respectively. The mean Γ of 2.5% quartile near the minimum is observed to perturb slightly and the mean Γ of 97.5% near the maximum is observed to shift slightly, all indicating an increased uncertainty exists in the results.

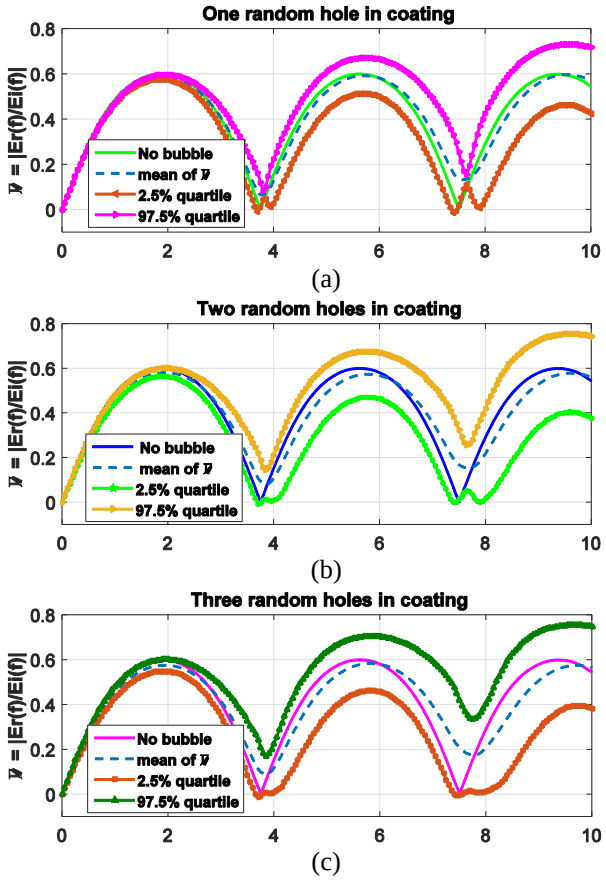

Fig. 14. The deviation in the mean and in 95% confidence intervals for Γ when the solution with stochastic holes is compared against the solution without holes: (a) one hole, (b) two holes, and (c) three holes.

Figure 15 (a) shows the mean of the Γ for the dielectric coating without holes by using the AM-DGTD method. The mean Γ with only one uncertain hole at the maximum 1.85 GHz are concentrated in the interval [0.581, 0.598], however, the values drop to range of [0.562, 0.597] and [0.544, 0.596] for the two and three holes, respectively, as shown in Figs. 15 (b)-(d). These numerical results are agreed with the physical explanation. In term of the value of the interval, we clearly see the smaller mean Γ have worse flaws corresponding to a larger number of holes.

From Fig. 16, it is clearly seen that the mean Γ at different frequencies is different for different numbers of random holes. For $0 \leq \Gamma \leq 0.4$, the values are increased with increasing of the number of the random hole; the $\Gamma = 0.5$ results slightly changed; and for $0.5 < \Gamma \leq 0.6$, the values are decreased with the increasing of the number of the random hole.

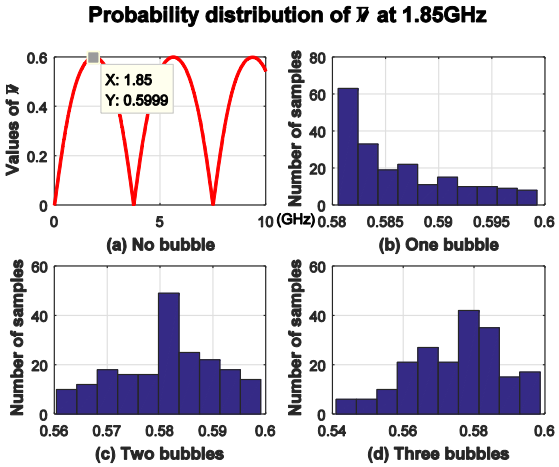

Fig. 15. Distribution of the reflection coefficient with different number of random holes: (a) the analytic solution of Γ without hole, (b) the distribution of Γ with one random hole at 1.85 GHz, (c) the distribution of Γ with two holes, and (d) the distribution of Γ with three random holes.

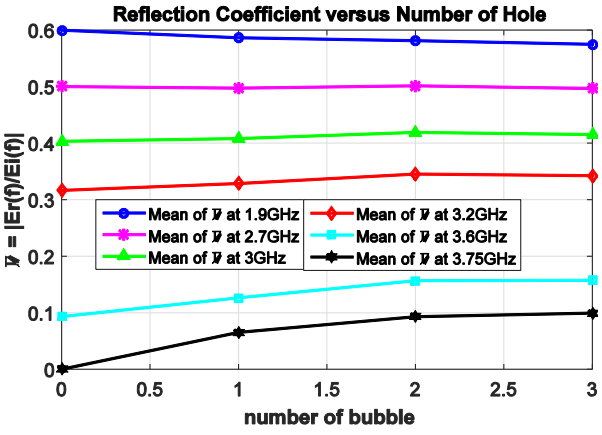

Fig. 16. The relationship between the mean of Γ and the number of hole.

V. CONCLUSION

In this paper, we discussed the use of an adaptive mesh integrated into discontinuous Galerkin method to research the impact of uncertain flaws in the 1D propagation problems. These sources of uncertain flaws are considered: the varied relative permittivity, thickness of coating and multivariable holes in the medium. The adaptive spatial discrete algorithm for the high order accurate DGTD method has been developed to solve

these irregular, complex, and random flaws in the dielectric coating.

The adaptive mesh technology, which generated by the displacement of nodes and the insertion of nodes, can provide efficient and optimum number of mesh elements as compared to simple uniform mesh. The simulation results have been shown that the new approach can save computational resources because of avoiding redundant division of the computational domain. Three typical experiments validate significant advantages of the AM-DGTD approach and show potential for further study of uncertain problems.

ACKNOWLEDGMENT

This work was supported in part by the Natural Science Foundation of China 61401199, Postgraduate Technology Innovation Project of Jiangsu Province KYLX15_0286, and the Technology key Project of the Education Department of Henan Province 14B413010.

REFERENCES

[1] D. Satas, A. A. Tracton, and A. J. Rafanelli, *Coatings Technology Handbook*. 2nd ed., Charleston Advisor, pp. 12-14, 2002.

[2] M. P. Schultz, "Effects of coating roughness and biofouling on ship resistance and powering," *Biofouling*, vol. 23, no. 5, pp. 331-341, Sep. 2007.

[3] L. R. A. X. De Menezes, A. Ajayi, *et al.*, "Efficient extraction of statistical moments in electromagnetic problems solved with the method of moments," in *Microwave and Optoelectronics Conference*, pp. 757-760, 2007.

[4] R. S. Edwards, A. C. Marvin, and S. J. Porter, "Uncertainty analyses in the finite-difference time-domain method," *IEEE Transactions on Electromagnetic Compatibility*, vol. 52, no. 1, pp. 155-163, Feb. 2010.

[5] A. C. M. Austin and C. D. Sarris, "Efficient analysis of geometrical uncertainty in the FDTD method using polynomial chaos with application to microwave circuits," *IEEE Transactions on Microwave Theory & Techniques*, vol. 61, no. 12, pp. 4293-4301, Sep. 2013.

[6] S. M. Smith and C. Furse, "Stochastic FDTD for analysis of statistical variation in electromagnetic fields," *IEEE Transactions on Antennas & Propagation*, vol. 60, iss. 7, pp. 3343-3350, May 2012.

[7] B. Navaneetha Raj, N. G. R. Iyengar, and D. Yadav, "Response of composite plates with random material properties using FEM and Monte-Carlo simulation," *Advanced Composite Materials*, vol. 7, no. 3, pp. 34-39, Apr. 2012.

[8] S. Sarkar and D. Ghosh, "A hybrid method for stochastic response analysis of a vibrating structure," *Archive of Applied Mechanics*, vol. 85, iss. 11, pp. 1607-1626, Nov. 2015.

[9] C. Chauvi, J. S. Hesthaven, and L. Lurati, "Computational modeling of uncertainty in time-domain electromagnetics," *Siam Journal on Scientific Computing*, vol. 28, no. 2, pp. 751-775, Jan. 2006.

[10] P. Li and L. J. Jiang, "Uncertainty quantification for electromagnetic systems using ASGC and DGTD method," *IEEE Transactions on Electromagnetic Compatibility*, vol. 57, no. 4, pp. 754-763, Feb. 2015.

[11] L. D. Angulo, J. Alvarez, *et al.*, "Discontinuous Galerkin time domain methods in computational electrodynamics: State of the art," *Forum for Electromagnetic Research Methods and Application Technologies*, vol. 10, no. 004, pp. 34-39, Aug. 2015.

[12] S. P. Gao, Y. Lu, and Q. Cao, "Hybrid method combining DGTD and TDIE for wire antenna-dielectric interaction," *Applied Computational Electromagnetics Society Journal*, vol. 60, no. 6, pp. 677-681, June 2015.

[13] H. Li, I. Hussain, Y. Wang, *et al.*, "Analysis the electromagnetic properties of dielectric coatings with uncertain flaws using DGTD method," *International Applied Computational Electromagnetics Society (ACES) Symposium*, Aug. 2017.

[14] L. Zhao, G. Chen, and W. Yu, "An efficient algorithm for SAR evaluation from anatomically realistic human head model using DGTD with hybrid meshes," *Applied Computational Electromagnetics Society Journal*, vol. 31, no. 6, pp. 629-635, June 2016.

[15] S. Yan and J. M. Jin, "A dynamic p-adaptation algorithm for the DGTD simulation of nonlinear EM-plasma interaction," *IEEE/ACES International Conference on Wireless Information Technology and Systems, IEEE*, pp. 1-2, May 2016.

[16] H. Edelsbrunner, *Geometry and Topology for Mesh Generation*. Cambridge University Press, 2001.

[17] L. Freitag and C. Ollivier-Gooch, "Tetrahedral mesh improvement using swapping and smoothing," *International Journal for Numerical Methods in Engineering*, vol. 40, no. 21, pp. 3979-4002, Mar. 1997.

[18] S. Swain, *Handbook of Stochastic Methods for Physics, Chemistry and the Natural Sciences*. Springer-Verlag, 1983.

[19] E. L. Bronaugh and J. D. M. Osburn, "A process for the analysis of the physics of measurement and determination of measurement uncertainty in EMC test procedures," in *Electromagnetic Compatibility*, pp. 245-249, Aug. 1996.

[20] D. L. Rumpf, *Statistics for Dummies*. John Wiley & Sons Inc., 2004.

[21] J. S. Hesthaven and T. Warburton, *Nodal Discontinuous Galerkin Methods: Algorithms, Analysis,*

and Applications. Springer Publishing Company, Incorporated, 2008.

[22] I. Hussain, H. Li, Y. Wang, and Q. Cao, "Modeling of structures using adaptive mesh in DGTD method for EM solver," presented at *Progress in Electromagnetics Research Symposium*, 2017.

[23] T. Warburton, "An explicit construction of interpolation nodes on the simplex," *Journal of Engineering Mathematics*, vol. 56, no. 3, pp. 247-262, Sep. 2006.

[24] R. Diehl, K. Busch, and J. Niegemann, "Comparison of low-storage Runge-Kutta schemes for discontinuous Galerkin time-domain simulations of Maxwell's equations," *Journal of Computational & Theoretical Nanoscience*, vol. 7, no. 8, pp. 1572-1580, Aug. 2010.

[25] G. Mur, "Absorbing boundary conditions for the finite-difference approximation of the time domain electromagnetic field equations," *IEEE Trans. Electromagnetic Compatibility*, vol. 23, no. 4, pp. 277-382, Nov. 1981.

Huiping Li received the master's degree in Communication and Information Systems from the Guangxi University, Guangxi, China, in 2007, and she is currently pursuing the Ph.D. degree in Electromagnetic Field and Microwave Technology from Nanjing University of Aeronautics and Astronautics, Nanjing, China, since 2014.

She has been a Lecturer with the School of Physics and Electronics, Henan University, Kaifeng, China, since 2008. Her current research interests include computational electromagnetism, wireless communication and circuit analysis.

Ishfaq Hussain received the B.Sc. degree in Electrical Engineering (Electronics & Communication) from the University of Engineering and Technology (UET) Lahore, Pakistan in 2008. He has been working on microwave systems as a Manager (Technical) with Pakistan-based public sector research and development organization since 2008. Currently, he is pursuing the M.Sc. degree at College of Electronic and Information Engineering, Nanjing University of Aeronautics and Astronautics, Nanjing China. His current research interests include computational electromagnetics and broadband microwave systems.

Yi Wang received the B.S. and Ph.D. degrees in Communication and Information System from Nanjing University of Aeronautics and Astronautics (NUAA), Nanjing, China in 2006 and 2012. After that, Wang joined the College of Electronic and Information Engineering, NUAA, as an assistant Professor.

His research interests includes computational electromagnetics, especially the finite-difference time-domain (FDTD) method, the FDTD modeling of the entire Earth-ionosphere system, the earthquake electromagnetics and radome design.

Qunsheng Cao received the Ph.D. degree in Electronic Engineering from The Hong Kong Polytechnic University, Hong Kong, in 2000. From 2000 to 2005, he was a Research Associate with the Department of Electrical Engineering, University of Illinois at Urbana-Champaign, and with the Army High Performance Computing Research Center (AHPCRC), University of Minnesota, respectively. In 2006, he joined the University of Aeronautics and Astronautics (NUAA), Nanjing, China, as a Professor of Electronic Engineering. He has authored or co-authored over 70 papers in refereed journals and conference proceedings. He has co-authored Multi-resolution Time Domain Scheme for Electromagnetic Engineering (Wiley, 2005).

His current research interests are in computational electromagnetism and antennas designs, particularly in time domain numerical techniques for the study of microwave devices and scattering applications.